Electrochemistry Communications 116 (2020) 106744

Contents lists available at ScienceDirect

Electrochemistry Communications

journal homepage: www.elsevier.com/locate/elecom

Measurement of the mass sensitivity of QCM with ring electrodes using electrodeposition

Jianguo Hu[a,b,*], Xianhe Huang[b], Song Xue[c], Göktug Yesilbas[a], Alois Knoll[a,*], Oliver Schneider[a]

[a] Institut für Informatik VI, Technische Universität München, München 85748, Germany
[b] School of Automation Engineering, University of Electronic Science and Technology of China, Chengdu 611731, China
[c] Physics of Energy Conversion and Storage, Technical University of Munich, Munich 85748, Germany

ARTICLE INFO

Keywords:
Quartz crystal microbalance (QCM)
Electrodeposition
Mass sensitivity measurement
Ring electrode QCM

ABSTRACT

A practical method for calculating the mass sensitivity of quartz crystal microbalance (QCM) resonators with ring-shaped Au electrodes on one side based on electrodeposition is presented in this communication. While for standard QCMs, an average mass sensitivity can be calculated despite its approximately Gaussian distribution, the mass sensitivity of QCMs with an asymmetrical electrode structure is difficult to calculate. However, non-standard electrode geometries might be beneficial for sensor applications especially in the area of electrochemistry. By measuring the resonance frequency change of a quartz crystal during deposition and applying Faraday's law, we determined the mass sensitivity of QCM resonators with a ring electrode. We also studied the influence of the gold electrode thicknesses on the mass sensitivity of the ring-shaped and disc shaped electrodes. The experimental results showed that the mass sensitivity of the ring-shaped electrodes was 5%~20% higher than those of the disc shaped electrodes. This method is practical and convenient for determining the mass sensitivity of the QCM with ring electrode, and it can be extended to measure QCMs with symmetrical and asymmetrical electrode structures. Such resonators with modified electrode structures may be of interest for studying electrochemical processes where a higher mass sensitivity is desirable.

1. Introduction

The quartz crystal microbalance (QCM) has been widely used in electrochemical processes for measuring small mass changes due to its high mass sensitivity and its low cost [1–3]. It has a simple structure; metal electrodes are plated on the upper and lower surfaces of the piezoelectric wafer. In 1959, Sauerbrey studied the relationship between the quartz crystal surface mass change Δm and the resonance frequency change Δf [4]:

$$\Delta f = f_R - f_0 = -\frac{2f_0^2}{\sqrt{\mu_q \rho_q}} \frac{\Delta m}{A} \tag{1}$$

f_R and f_0: resonance frequency of quartz crystal with and without mass loading; A: sensing area; μ_q: shear modulus of AT-cut quartz crystal ($\mu_q = 2.947 \times 10^{11}\ g\ cm^{-1}\ s^{-2}$); ρ_q: quartz density ($\rho_q = 2.643\ g\ cm^{-3}$). This equation describing the mass sensitivity of QCM resonators with disc shaped electrodes on both sides laid the theoretical foundation for the application of QCMs.

The QCM can be operated in liquids and therefore it is possible to apply the Sauerbrey's equation in electrochemistry for deposition processes and other reactions involving mass changes at the electrode, provided that the deposited layer is acoustically thin, rigidly bound, and smooth [5]. An equivalent circuit model was introduced to describe the relationship between electrical impedance and surface loads [6]. These models have been expanded to include also the behavior of non-rigidly bound viscoelastic films or rough layers [7,8]. After more than sixty years of development, the QCMs have been widely applied in electrochemistry, electrochemical surface science and sonoelectrochemistry and so on [9–12].

There are two reasons that make the mass sensitivity for resonators with arbitrary electrode shape difficult to calculate. One is that the mass sensitivity is not constant but rather characterized by an approximately Gaussian distribution [13] even for standard electrode configurations, and the other is that additional complications arise when QCMs with differently shaped electrodes are used. The geometry of the electrode is closely related to the mass sensitivity of the QCM [14–17]. For example, Y. Lee [14] investigated the electrical loading sensing mechanism of QCM, C. Zhang [15,16] found that a QCM transducer with an asymmetric electrode structure shows an improved mass sensitivity comparing to a standard electrode QCM, and Y. Yao [17] developed

* Corresponding authors at: Institut für Informatik VI, Technische Universität München, München 85748, Germany.
E-mail addresses: jianguo.hu@tum.de (J. Hu), knoll@mytum.de (A. Knoll).

https://doi.org/10.1016/j.elecom.2020.106744
Received 20 April 2020; Received in revised form 4 May 2020; Accepted 11 May 2020
Available online 18 May 2020

humidity sensors using QCM transducer with asymmetric electrode structures. Therefore, it might be beneficial for certain applications to use tailored electrode shapes.

In this work, we applied a well-established method [18] for experimentally determining the mass sensitivity of a QCM to QCM quartzes with ring-shaped electrodes on one side. Choosing quartzes with ring electrodes were motivated by earlier work in gas phase deposition experiments that showed that the ring electrode QCMs' mass sensitivity distribution is approximately uniform [19]. By measuring Δf of a quartz crystal caused by deposition of a thin copper film and applying Faraday's law, we calculated the mass sensitivity of the QCM with ring electrode. Besides, we carried out AFM measurements to investigate the roughness of the thin copper films, and we used XRD to verify the composition of the thin films. The experimental results showed that the mass sensitivity of the QCM with the ring-shaped electrode, in the following called "ring" electrodes, facing the electrolyte (i.e. the "upper" electrode in our experimental configuration) was 5%~20% higher than those of the disc shaped ("disc") electrodes. Naturally, the mass sensitivity of the electrode exposed to the electrolyte is also influenced by the geometrical shape of the electrode on the rear side of the quartz ("lower" electrode), as only the region between both electrodes contributes to the mass sensitivity. Such resonators with modified electrode structures maybe special interest for studies in electrochemical energy storage, where first interesting results with standard quartzes in the past years showed a rather complex response that is not purely gravimetric [20,21].

2. Experimental section

2.1. Specifications of the QCM resonators with ring electrodes

The electrode shape has an important influence on the performance of QCMs, and its mass sensitivity is the key factor for practical application of QCMs [22]. We designed QCM quartzes with ring electrode structures on one side to improve the performance of QCMs. Quartz plates with a fundamental frequency of 10 MHz and a diameter of 8.7 mm were applied in the experiments, and the outer diameter d_1 of the electrodes evaporated onto the quartz was 5.1 mm (Wintron Electronic Co., Ltd. Zhengzhou City, China). Fig. 1 shows the geometry of these resonators. In this study, we varied the electrode thickness T_E (500 Å, 1000 Å, 1500 Å and 2000 Å). The thickness of the ring electrode and the disc electrode of the same resonator are the same. We marked the QCMs with 500 Å, 1000 Å, 1500 Å and 2000 Å thickness electrodes as group A, B, C and D, respectively.

2.2. Electrodeposition based on Faraday's law of electrolysis

The Sauerbrey's equation can calculate the mass sensitivity of the QCM with disc shaped electrodes. However, it is quite hard to calculate the mass sensitivity of the QCM with ring electrode. We propose electrodeposition, based on Faraday's law of electrolysis, to solve this difficulty. This method is actually often used even for standard QCM quartzes to perform an experimental calibration instead of just using the theoretical values [23–25]. The schematic diagram of the experimental setup for copper electrodeposition is shown in Fig. 2.

In this work, we applied chronoamperometry to deposit a thin copper film on the electrode surface. The electrolyte (100 ml) was composed of 0.01 M $CuSO_4{\cdot}5H_2O$, 0.1 M Na_2SO_4 and 5 mM H_2SO_4. The quartz electrode under study (ring or disc) faced the electrolyte and served as the working electrode (WE), while the other electrode was insulated from the electrolyte via a sealing O-ring. A Pt wire was used as the counter electrode (CE), and a $Hg/Hg_2SO_4/0.6$ M K_2SO_4 electrode as the reference electrode (RE), to which all potentials are referred to in this communication. The potential of the RE with respect to NHE is +0.658 V. Copper deposition was carried out at room temperature (25 °C). The electrolyte was deaerated with Ar purging before and between the experiments. During the experiments, an overflow of Ar was maintained to prevent oxygen from entering the electrolyte and lowering the current efficiency. First, cyclic voltammograms (CVs) were recorded at a potential scan rate of 5 mV/s. The deposition potential of −0.465 V was selected based on the analysis of these CVs. Copper films were potentiostatically electrodeposited on ten quartzes (5 with ring electrodes as upper electrodes and 5 with disc electrodes as upper electrodes) in each group for one hour. The principle is governed by the Faraday's law [26] as follows:

$$m = \frac{Q \cdot M}{F \cdot z} \tag{2}$$

$$Q = \int_0^t Idt \tag{3}$$

where m is the mass of copper deposited on the electrode in grams, Q is the total electric charge passing through the cell in coulombs, F = 96485 C/mol is the Faraday constant, M is the molar mass of copper in grams per mol, and z is the valency number of the Cu ions (i.e. z = 2). I is the time-dependent current of the copper deposition process, and t is the total time of deposition.

It is worth noting that there might be detachment issues for the Au electrode on quartz in contact with electrolyte. However, there is a chromium adhesive layer underneath the Au electrode, which enhances the adhesion of the electrode. The situation is not so much different from standard EQCM quartzes, just that the interface line to the electrolyte is longer for a ring electrode structure QCM. In our experiments, the quartzes typically were operated for a full day, and within that period of time, no indication of delamination was seen. After electrodeposition, the mass sensitivity of QCM with ring electrode is calculated

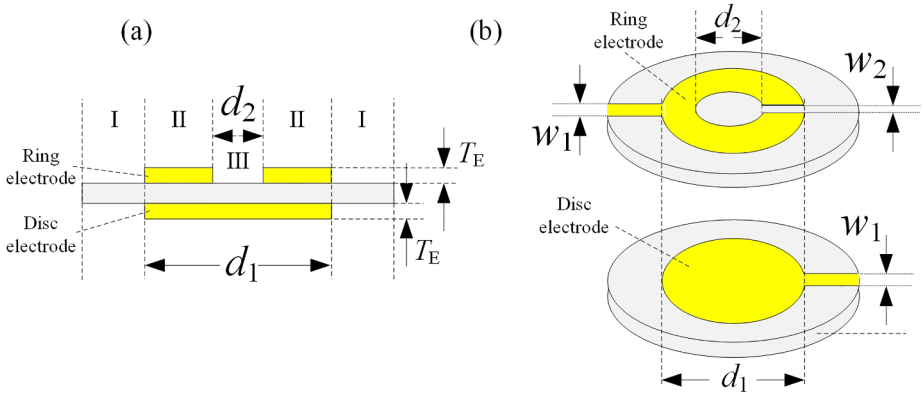

Fig. 1. Schematic diagram of the QCM resonators with a ring electrode on one side. (a) Cross section; I, II, and III represent quartz areas without electrode layer on either side, with an electrode layer on both sides, and an electrode layer on one side only, respectively. The ring and disc electrodes have the same thickness T_E; d_1(d_1 = 5.1 mm), d_2(d_2 = 2 mm) are the outer and inner diameters of the ring electrode. (b) 3D view of the resonators. The upper figure shows the side with the ring electrode, the lower one the side with a disc electrode. W_1 (W_1 = 0.5 mm) and W_2 (W_2 = 0.3 mm) represent the width of the electrode contact pads and an opening in the ring structure (because of manufacturing restrictions, a circular mask was needed to cover the internal part of the ring, and this circular mask had to be connected to other parts through a mechanical beam.), respectively.

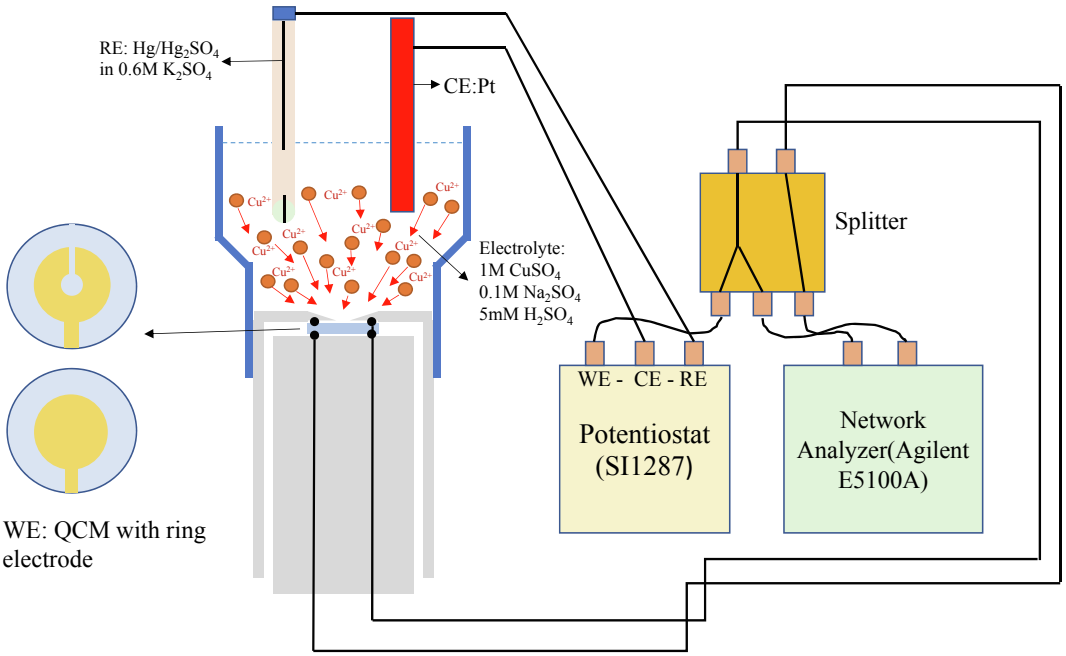

Fig. 2. Schematic diagram of the electrodeposition setup. An Electrochemical Interface SI1287 (Solartron) was used as potentiostat, and a network analyzer (NA) E5100A from Agilent to measure in parallel to the electrochemical measurement the quartz admittance spectra in the vicinity of the resonance frequency. A splitter box was used to couple the upper electrode of the QCM resonator with both the potentiostat and the NA via an inductor and a capacitor, respectively, to prevent interference of the two instruments with each other. The measured real part of the admittance was fitted to a Lorentzian function. The center frequency of the fit equals f_R, and the full width at half maximum the so-called dampening w.

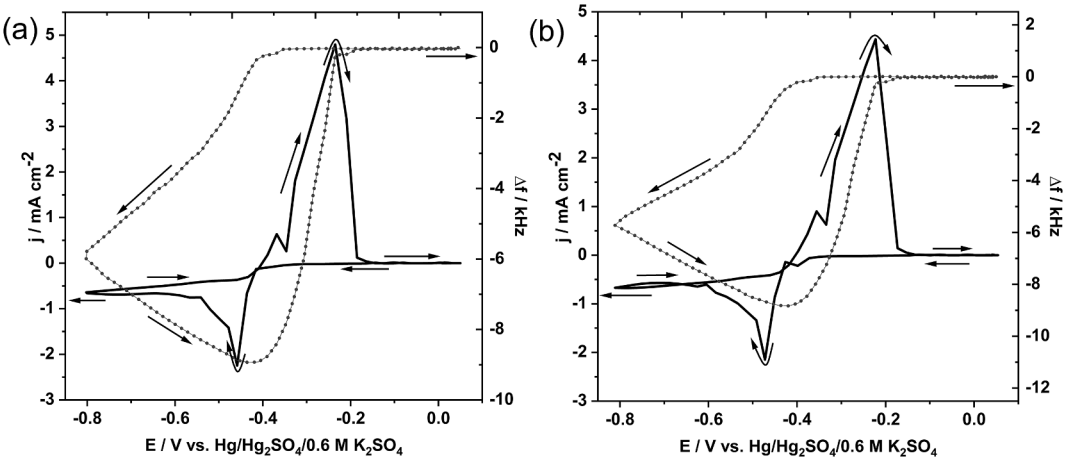

Fig. 3. Current densities (lines) and related frequency changes (dots) during deposition and dissolution of Cu from 0.01 M $CuSO_4{\cdot}5H_2O$, 0.1 M Na_2SO_4 and 5 mM H_2SO_4 at a scan-rate of 5 mV/s. (a) Ring electrode as WE; (b) Disc electrode as WE.

by,

$$S = \frac{m}{\Delta f \cdot A} \tag{4}$$

where m is the mass of the Cu film calculated from Eqs. (2) and (3), Δf is the integral change of the resonance frequency during deposition, A is the electrochemically active electrode area for Cu deposition. A is 0.191 cm^2 or 0.222 cm^2 for the ring and disc sides as upper electrodes, respectively.

2.3. AFM characterization of the thin films

The roughness of the thin copper films is a key index of deposition. In the experiment, we needed to ensure the uniformity of the coating. After the thin films were deposited on the electrodes, we used atomic force microscopy (AFM) [27,28], choosing a multimode EC-STM/AFM instrument (Veeco Instrument, Inc.) with a Nanoscope IIID controller and the Nanoscope 5.31rl software [29] (AFM tips, Bruker RTESP-300.) to investigate the thin film morphology.

2.4. X-ray diffraction analysis

X-ray diffraction (XRD) [30,31] of the thin films deposited on the electrodes was carried out by X'Pert (Malvern Panalytical Ltd., the Netherland) to investigate the composition. The XRD measurements were executed in a 2θ range of 5–90°, in steps of 0.0472°(2θ), and 1s integration time per step (Bragg-Brentano geometry with fixed divergence slits, continuous mode, position sensitive detector, Cu Kα radiation).

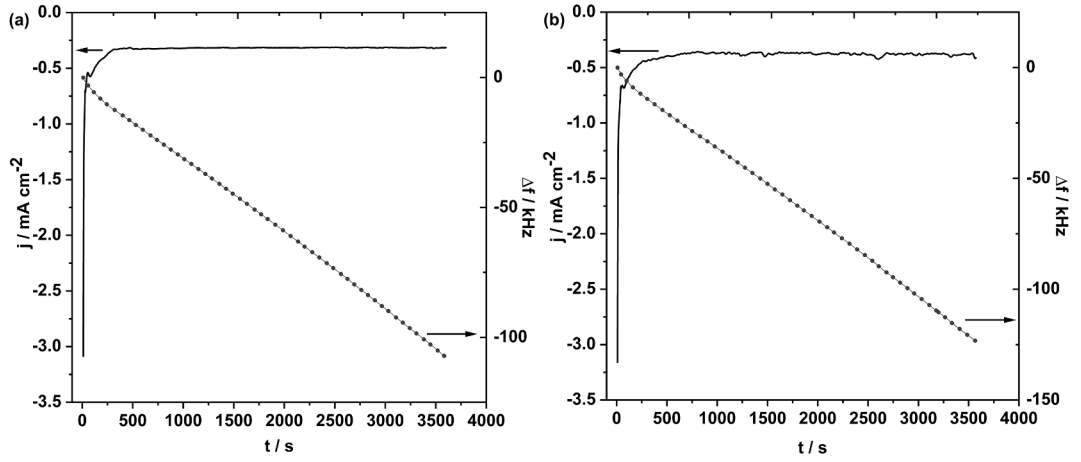

Fig. 4. Current transients measured in deaerated 0.01 M $CuSO_4 \cdot 5H_2O$, 0.1 M Na_2SO_4 and 5 mM H_2SO_4 during the potentiostatic electrodeposition of Cu at an applied potential of −0.458 V vs. $Hg/Hg_2SO_4/0.6$ M K_2SO_4. (a) Ring electrode as WE; (b) Disc electrode as WE.

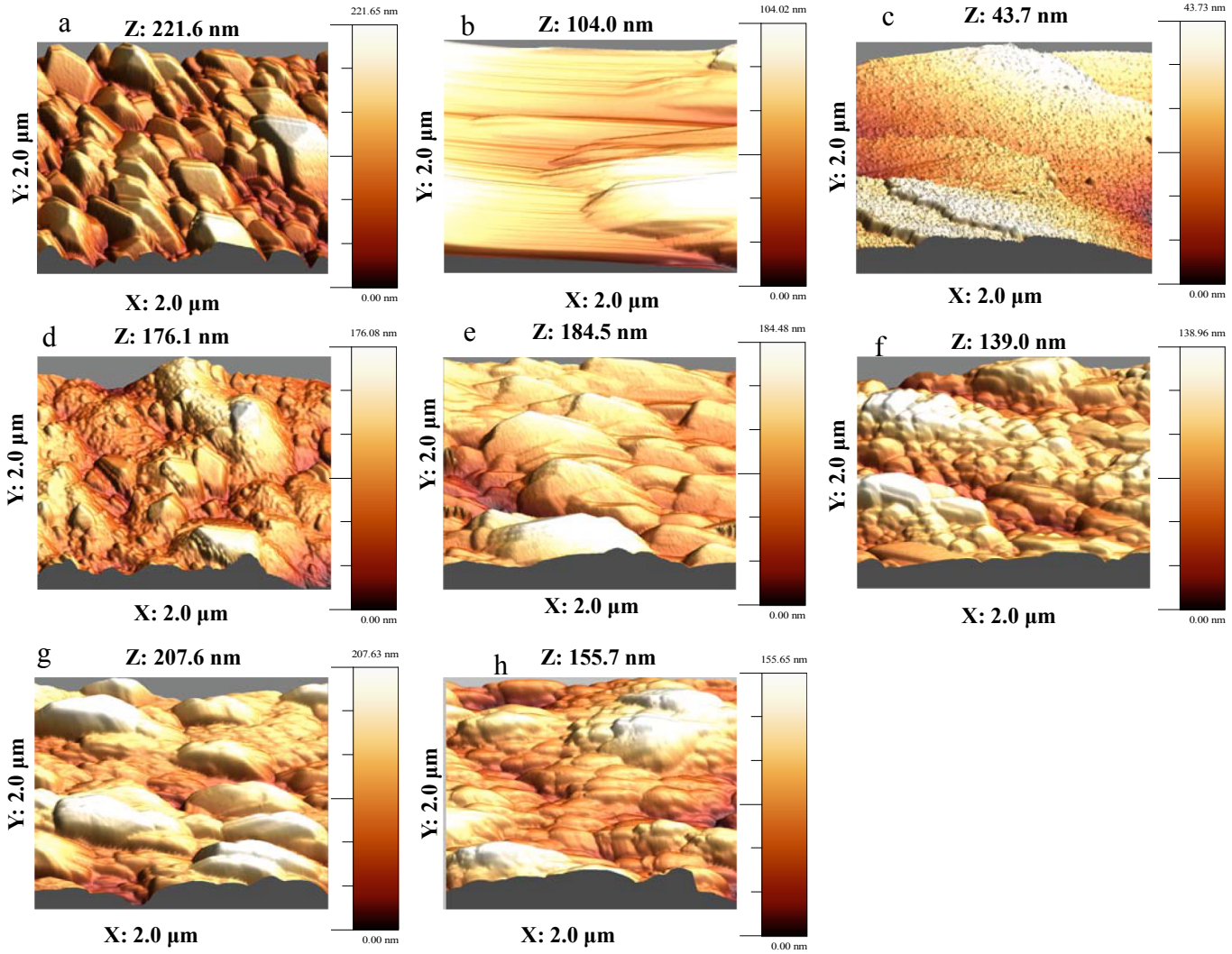

Fig. 5. AFM images of the measurement points of thin Cu films deposited on the surface of the QCM resonators. Group A: (a) and (b) are ring and disc electrodes (T_E = 500 Å), respectively; Group B: (c) and (d) are ring and disc electrodes (T_E = 1000 Å), respectively; Group C: (e) and (f) are ring and disc electrodes (T_E = 1500 Å), respectively; Group D: (g) and (h) are ring and disc electrodes (T_E = 2000 Å), respectively.

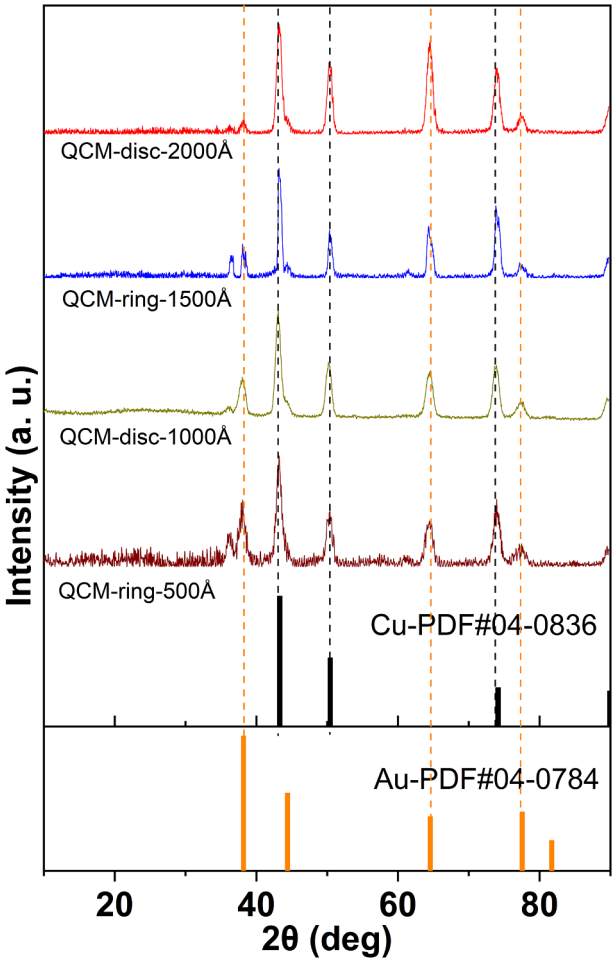

Fig. 6. XRD measurement of the electrodes of the QCM resonators after electrodeposition.

3. Results and discussion

3.1. Cyclic electrodeposition and potentiostatic electrodeposition of Cu

The potential sweep was started at +0.055 V for the study of the electrodeposition of Cu on Au electrode, and swept down to −0.813 V vs. Hg/Hg_2SO_4/0.6 M K_2SO_4. The general shape of the CVs looks as expected for Cu electrodeposition at a polycrystalline Au electrode [32]. For the ring electrode facing the electrolyte (Fig. 3a), a first cathodic process is apparent in the cyclic voltammogram (CV) when the potential becomes lower than −300 mV. This cathodic process was connected to a slight frequency change (−350 Hz), and corresponds to Cu underpotential deposition on Au. The bulk electrodeposition process starts at $E < -0.4$ V, with a strong decrease in the f_R accompanying the increase in cathodic currents. The f_R continued to decrease in the beginning of the backsweep, as the current density j remained negative. At $E > -0.407$ V the currents became positive, and the dissolution of the copper caused the frequency to start increasing. For a disc electrode facing the electrolyte (Fig. 3b), the electrodeposition and dissolution processes are basically the same as in Fig. 3a.

The Cu films on the surface of the ring electrode and the disc electrode were obtained by potentiostatic electrodeposition at −0.458 V vs. Hg/Hg_2SO_4/0.6 M K_2SO_4. Fig. 4 shows that the current decreases rapidly at the beginning of electrodeposition and then decreases slowly over time until a nearly constant value is reached. Correspondingly, the f_R first showed a rapid decrease and then decreased linearly with time.

3.2. Characterization of the thin copper films

Fig. 5 shows the characterization of the AFM surface analysis of the thin copper films deposited on the electrodes. It should be noted that as the whole electrode surface was coated, it is impossible to measure the entire surface region with AFM. Thus, for each ring and disc electrode, we chose two symmetrical regions near the edge of the deposited film as the measurement points. More details are included in the Supporting information (Figs. S1 and S2). For examples, the average roughnesses of the two symmetrical measurement points of one disc electrode (electrode thickness T_E = 2000 Å) are 23.6 nm and 24.4 nm, respectively; the average roughnesses of the ones of one ring electrode (electrode thickness T_E = 500 Å) are 35.2 nm and 33.9 nm, respectively. Namely, the two symmetrical regions on each electrode always give similar roughness. Therefore, only one such region for each selected electrode is shown in Fig. 5. In general, for the average roughness of the measuring area, under the same electrode thickness, the average roughness of the measuring region of the ring electrode is larger than that of the disc electrode. The average roughnesses of the measuring regions are 27.6 nm, 12.4 nm, 6.9 nm, 20.4 nm, 23.6 nm, 19.6 nm, 30.4 nm and 24.4 nm for ring and disc electrode of the QCM with T_E = 500 Å, 1000 Å, 1500 Å and 2000 Å, respectively. The average roughness of the measuring region Cu films was calculated mainly from those area covered with Cu films. These AFM images revealed that all the measured areas exhibited a uniform morphology.

3.3. XRD measurement analysis

The XRD measurement of several Cu films deposited on various QCM resonators after electrodeposition is shown in Fig. 6. Three well-defined peaks at 43.1774°, 50.3431°, and 73.8183° are assigned to the (1 1 1), (2 0 0), and (2 2 0) planes of the Cu metal phase, respectively; the other three well-defined peaks appearing at 38.2256°, 64.4256°, and 77.3291° belong to the (1 1 1), (2 2 0) and (3 1 1) planes of the Au substrate, respectively, because the Cu thin films are grown on Au

Table 1
The mass sensitivity of different electrode thickness of QCM with ring electrode.

Type	A(500 Å)		B(1000 Å)		C(1500 Å)		D(2000 Å)	
	Ring	Disc	Ring	Disc	Ring	Disc	Ring	Disc
$S(10^{-9}$ g/cm²·Hz)	4.77	4.24	4.14	3.89	4.56	3.78	4.58	4.23
	4.31	4.23	4.40	3.97	4.37	4.04	4.53	4.19
	4.51	4.16	4.59	3.59	4.03	3.96	4.17	4.09
	4.78	3.83	4.78	3.91	3.75	3.77	3.97	3.89
	4.30	4.07	4.65	3.71	4.30	3.89	4.27	4.09
$S(S_{Ring}$ or $S_{Disc})$	4.53	4.10	4.51	3.81	4.20	3.89	4.29	4.09
δ	0.24	0.17	0.25	0.16	0.32	0.12	0.24	0.14
$\bar{S}_{CRI}$	110.5%		118.4%		108.0%		105.1%	

electrodes. This reveals that the surface of the thin copper film is composed of copper crystallites, as expected. There is no indication of significant oxidation or impurities.

3.4. Mass sensitivity of the QCM resonators with ring electrode

After the one-hour deposition, the mass sensitivity in Table 1 is obtained from Eqs. (2)–(4). S, $\bar{S}$($\bar{S}_{Ring}$ or $\bar{S}_{Disc}$), δ and $\bar{S}_{CRI}$ are mass sensitivity, average mass sensitivity, standard error and comparative relative indicators, respectively. The results presented for group A, B, C and D are each based on deposition of Cu films on the ring electrodes of five different QCM resonators and on the disc electrodes of (another) five different QCM resonators with the same specifications (electrode geometry and thickness). The average mass sensitivity of group A, B, C and D are 4.53×10^{-9} g/cm^2·Hz ($\bar{S}_{Ring}$) and 4.10×10^{-9} g/cm^2·Hz ($\bar{S}_{Disc}$), 4.51×10^{-9} g/cm^2 Hz ($\bar{S}_{Ring}$) and 3.81×10^{-9} g/cm^2·Hz ($\bar{S}_{Disc}$), 4.19×10^{-9} g/cm^2·Hz ($\bar{S}_{Ring}$) and 3.89×10^{-9} g/cm^2·Hz ($\bar{S}_{Disc}$), 4.29×10^{-9} g/cm^2·Hz ($\bar{S}_{Ring}$) and 4.09×10^{-9} g/cm^2·Hz ($\bar{S}_{Disc}$), respectively. Totally, $\bar{S}_{Ring} > \bar{S}_{Disc}$ shows that the ring electrodes in each group show an enhanced mass sensitivity comparing to the disc electrode for the same electrode thickness. The comparative relative indicators ($\bar{S}_{CRI} = \bar{S}_{Ring}/\bar{S}_{Disc}$) of the average mass sensitivity of the ring electrodes are 10.5%, 18.4%, 8.1%, and 5.1% higher than those of the disc electrodes for the ring electrode QCM with a thickness of 500 Å, 1000 Å, 1500 Å and 2000 Å. These are in agreement with our earlier study [19] showing that the ring electrode QCM has an approximately uniform mass sensitivity distribution. The approximately uniform mass sensitivity distribution then can contribute to the integrated mass sensitivity of the ring electrode side being greater than that of the disc electrode side.

The best standard error and maximum standard error are 0.12×10^{-9} g/cm^2·Hz and 0.32×10^{-9} g/cm^2·Hz, respectively. These low standard errors show the reliability of the experimental system and the good stability.

Table 1 shows also that the thinner the Au electrode, the higher is the mass sensitivity. According to our previous study, the higher resonance frequency results in a higher mass sensitivity [33]. This is the same behavior known from the Sauerbrey's equation for standard resonators. In the factual measurement, the average resonance frequencies of group A, B, C and D decreased gradually. These results are consistent with our previous research results [33].

4. Conclusion

In this communication, we have applied a practical method for calculating the mass sensitivity of quartz resonators with ring electrodes on one side based on electrodeposition. The experimental results showed that the mass sensitivity of the ring electrodes was 5%～20% higher than those of the disc electrodes. This method is very helpful for determining the mass sensitivity of the QCM with such ring electrodes, and it can be extended to measure QCMs with symmetrical and asymmetrical electrode structures. Such resonators with modified electrode structures may be of interest for studying electrochemical processes where a higher mass sensitivity is desirable. More detailed theoretical and experimental studies are required to lay the base for application to non-rigid systems and in more complex media like ionic liquids. This maybe of special interest for studies in electrochemical energy storage, where first interesting results with standard quartzes in the past years showed a rather complex response that is not purely gravimetric.

CRediT authorship contribution statement

Jianguo Hu: Writing - original draft, Conceptualization, Data curation, Funding acquisition, Investigation, Methodology. **Xianhe Huang:** Validation. **Song Xue:** Formal analysis, Investigation. **Göktug Yesilbas:** Formal analysis. **Alois Knoll:** Resources, Supervision. **Oliver Schneider:** Supervision, Validation, Project administration, Writing - review & editing.

Declaration of Competing Interest

The authors declare that they have no known competing financial interests or personal relationships that could have appeared to influence the work reported in this paper.

Acknowledgements

This work was supported by the Technical University of Munich (TUM) in the framework of the Open Access Publishing Program. Jianguo Hu would like to thank the China Scholarship Council (CSC) for supporting him in conducting research at the Technical University of Munich in Germany. He would also like to express his appreciation to many people who helped with this work, especially Prof. Dr. Aliaksandr Bandarenka, Dr. Lukas Seidl, Dr. Sladjana Martens, and Mr. Shujin Hou. We thank Prof. Dr. Holger Fritze (TU Clausthal) for the use of his automatic fitting software for fitting of the admittance spectra.

Appendix A. Supplementary data

Supplementary data to this article can be found online at https://doi.org/10.1016/j.elecom.2020.106744.

References

[1] S. Bruckenstein, M. Shay, Experimental aspects of use of the quartz crystal microbalance in solution, Electrochim. Acta 30 (1985) 1295–1300.
[2] O. Melroy, K. Kanazawa, J.G. Gordon II, D. Buttry, Direct determination of the mass of an underpotentially deposited monolayer of lead on gold, Langmuir 2 (1986) 697–700.
[3] Y. Ratieuville, P. Viers, J. Alexandre, G. Durand, A new electrochemical cell adapted to quartz crystal microbalance measurements, Electrochem. Commun. 2 (2000) 839–844.
[4] G. Sauerbrey, Use of quartz vibration for weighing thin films on a microbalance, Z. Phys. 155 (1959) 206–222.
[5] K.K. Kanazawa, J. Gordon, Frequency of a quartz microbalance in contact with liquid, Anal. Chem. 57 (1985) 1770–1771.
[6] H.L. Bandey, S.J. Martin, R.W. Cernosek, A.R. Hillman, Modeling the responses of thickness shear mode resonators under various loading conditions, Anal. Chem. 71 (1999) 2205–2214.
[7] S.J. Martin, V.E. Granstaff, G.C. Frye, Characterization of a quartz crystal microbalance with simultaneous mass and liquid loading, Anal. Chem. 63 (1991) 2272–2281.
[8] E. Tellechea, D. Johannsmann, N.F. Steinmetz, R.P. Richter, I. Reviakine, Model-independent analysis of QCM data on colloidal particle adsorption, Langmuir 25 (2009) 5177–5184.
[9] Y. Liu, X. Yu, R. Zhao, D.S. Guan, Z. Bo, G. Liu, Quartz crystal biosensor for real time monitoring of molecular recognition between protein and small molecular medicinal agents, Biosens. Bioelectron. 19 (2003) 9–19.
[10] K. Reimhult, K. Yoshimatsu, K. Risveden, S. Chen, L. Ye, A. Krozer, Characterization of QCM sensor surfaces coated with molecularly imprinted nanoparticles, Biosens. Bioelectron. 23 (2008) 1908–1914.
[11] P. Sakkas, O. Schneider, S. Martens, P. Thanou, G. Sourkouni, C. Argirusis, Fundamental studies of sonoelectrochemical nanomaterials preparation, J. Appl. Electrochem. 42 (2012) 763–777.
[12] S. Shi, S. Reisberg, G. Anquetin, V. Noël, M.C. Pham, B. Piro, General approach for electrochemical detection of persistent pharmaceutical micropollutants: application to acetaminophen, Biosens. Bioelectron. 72 (2015) 205–210.
[13] M.D. Ward, E.J. Delawski, Radial mass sensitivity of the quartz crystal microbalance in liquid media, Anal. Chem. 63 (1991) 886–890.
[14] Y. Lee, D. Everhart, F. Josse, The quartz crystal resonator as detector of electrical loading: an analysis of sensing mechanisms, Proc. IEEE Int. Frequency Control Symp. (1996) 577–585.
[15] C. Zhang, J.F. Vetelino, Bulk acoustic wave sensors for sensing measurand-induced electrical property changes in solutions, IEEE. Trans. Ultrason. Ferroelectr. Freq. Control 48 (2001) 773–778.
[16] C. Zhang, J.F. Vetelino, Chemical sensors based on electrically sensitive quartz resonators, Sen. Act. B: Chem. 91 (2003) 320–325.
[17] Y. Yao, X.H. Huang, B.Y. Zhang, Z. Zhang, D. Hou, Z.K. Zhou, Facile fabrication of high sensitivity cellulose nanocrystals based QCM humidity sensors with asymmetric electrode structure, Sen. Act. B: Chem. 302 (2020) 127192.
[18] M. Hepel, S. Bruckenstein, Tracking anion expulsion during underpotential deposition of lead at silver using the quartz microbalance, Electrochim. Acta 34 (1989) 1499–1504.

[19] X.H. Huang, Q.S. Bai, P. Wei, J.G. Hu, Quartz crystal microbalance with approximately uniform sensitivity distribution, Anal. Chem. 90 (2018) 6367–6370.
[20] L. Seidl, N. Bucher, E. Chu, S. Hartung, S. Martens, O. Schneider, U. Stimming, Intercalation of solvated Na-ions into graphite, Energy Environ. Sci. 10 (2017) 1631–1642.
[21] N. Shpigel, M.D. Levi, S. Sigalov, L. Daikhin, D. Aurbach, In situ real-time mechanical and morphological characterization of electrodes for electrochemical energy storage and conversion by electrochemical quartz crystal microbalance with dissipation monitoring, Acc. Chem. Res. 51 (2018) 69–79.
[22] X.F. Wang, B. Ding, M. Sun, J.Y. Yu, G. Sun, Nanofibrous polyethyleneimine membranes as sensitive coatings for quartz crystal microbalance-based formaldehyde sensors, Sen. Act. B: Chem. 144 (2010) 11–17.
[23] R. Seakr, Microstructure and crystallographic characteristics of nanocrystalline copper prepared from acetate solutions by electrodeposition technique, Trans. Nonferrous Met. Soc. China 27 (2017) 1423–1430.
[24] T.A. Green, P. Valverde, S. Roy, Anodic reactions and the corrosion of copper in deep eutectic solvents, J. Electrochem. Soc. 165 (2018) 313–320.
[25] O. Ghodbane, L. Roué, D. Bélanger, Copper electrodeposition on pyrolytic graphite electrodes: effect of the copper salt on the electrodeposition process, Electrochim. Acta 52 (2007) 5843–5855.
[26] D.R. Gabe, Coulometric techniques for surface coatings, Trans. IMF 77 (1999) 213–217.
[27] N. Kaiser, Review of the fundamentals of thin-film growth, Appl. Opt. 41 (2002) 3053–3060.
[28] I.D. Kim, Y. Avrahami, H.L. Tuller, Y.B. Park, M.J. Dicken, H.A. Atwater, Study of orientation effect on nanoscale polarization in BaTiO3 thin films using piezo with ring electrodesponse force microscopy, Appl. Phys. Lett. 86 (2005) 192907.
[29] I. Horcas, R. Fernández, J.M. Gómez-Rodríguez, J. Colchero, J. Gómez-Herrero, A.M. Baro, WSXM: a software for scanning probe microscopy and a tool for nanotechnology, Rev. Sci. Instrum. 78 (2007) 013705.
[30] M. Yang, Z. Guo, L.N. Li, Y.Y. Huang, J.H. Liu, Q. Zhou, X. Chen, X.J. Huang, Electrochemical determination of arsenic (III) with ultra-high anti-interference performance using Au–Cu bimetallic nanoparticles, Sen. Act. B: Chem. 231 (2016) 70–78.
[31] M.R. Mahboob, Z.H. Zargar, T. Islam, A sensitive and highly linear capacitive thin film sensor for trace moisture measurement in gases, Sen. Act. B: Chem. 228 (2016) 658–664.
[32] O. Schneider, S. Matić, C. Argirusis, Application of the electrochemical quartz crystal microbalance technique to copper sonoelectrochemistry Part 1. Sulfate-based electrolytes, Electrochim. Acta 53 (2008) 5485–5495.
[33] X.H. Huang, Q.S. Bai, J.G. Hu, D. Hou, A practical model of quartz crystal microbalance in actual applications, Sensors 17 (2017) 1785.